

# Strong mechanical driving of a single electron spin

A. Barfuss<sup>1†</sup>, J. Teissier<sup>1†</sup>, E. Neu<sup>1</sup>, A. Nunnenkamp<sup>1,2</sup> and P. Maletinsky<sup>1\*</sup>

**Quantum devices for sensing and computing applications require coherent quantum systems, which can be manipulated in fast and robust ways<sup>1</sup>. Such quantum control is typically achieved using external electromagnetic fields, which drive the system's orbital<sup>2</sup>, charge<sup>3</sup> or spin<sup>4,5</sup> degrees of freedom. However, most existing approaches require complex and unwieldy gate structures, and with few exceptions<sup>6,7</sup> are limited to the regime of weak coherent driving. Here, we present a novel approach to coherently drive a single electronic spin using internal strain fields<sup>8–10</sup> in an integrated quantum device. Specifically, we employ time-varying strain in a diamond cantilever to induce long-lasting, coherent oscillations of an embedded nitrogen-vacancy (NV) centre spin. We perform direct spectroscopy of the phonon-dressed states emerging from this drive and observe hallmarks of the sought-after strong-driving regime<sup>6,11</sup>, where the spin rotation frequency exceeds the spin splitting. Furthermore, we employ our continuous strain driving to significantly enhance the NV's spin coherence time<sup>12</sup>. Our room-temperature experiments thereby constitute an important step towards strain-driven, integrated quantum devices and open new perspectives to investigate unexplored regimes of strongly driven multilevel systems<sup>13</sup> and exotic spin dynamics in hybrid spin-oscillator devices<sup>14</sup>.**

The use of crystal strain for the manipulation of single quantum systems ('spins') in the solid state brings vital advantages compared to established methods relying on electromagnetic fields. Strain fields can be straightforwardly engineered in the solid state and can offer a direct coupling mechanism to embedded spins<sup>8,15</sup>. As they are intrinsic to these systems, strain fields are immune to drifts in the coupling strength. Also, strain does not generate spurious stray fields, which are unavoidable with electric or magnetic driving and can cause unwanted dephasing or heating of the environment. Furthermore, coupling spins to strain offers attractive features of fundamental interest. For instance, strain can be used to shuttle information between distant quantum systems<sup>15</sup>, and has been proposed to generate squeezed spin ensembles<sup>14</sup> or to cool mechanical oscillators to their quantum ground state<sup>16</sup>. These attractive perspectives for strain-coupled hybrid quantum systems motivated recent studies of the influence of strain on nitrogen-vacancy (NV) centre electronic spins<sup>9,10,17</sup> and experiments on strain-induced, coherent driving of large NV spin ensembles<sup>8</sup>. Promoting such experiments to the single-spin regime, however, remains an outstanding challenge, and would constitute a major step towards the implementation of integrated, strain-driven quantum systems.

Here, we demonstrate the coherent manipulation of a single electronic spin using time-periodic, intrinsic strain fields generated in a single-crystalline diamond mechanical oscillator. We show that such strain fields allow us to manipulate the spin in the strong-driving regime, where the spin manipulation frequency significantly exceeds the energy splitting between the two involved spin states,

and to protect the spin from environmental decoherence. Our experiments were performed on electronic spins in individual NV lattice point defect centres, embedded in single-crystalline diamond cantilevers. The negatively charged NV centres we studied have a spin  $S=1$  ground state with basis states  $\{|0\rangle, |-1\rangle, |+1\rangle\}$ , where  $|m_s\rangle$  is an eigenstate of the spin operator  $\hat{S}_z$  along the NV's symmetry axis,  $z$  (Fig. 1a). The energy difference between  $|\pm 1\rangle$  and  $|0\rangle$  is given by the zero-field splitting  $D_0=2.87$  GHz. The levels  $|\pm 1\rangle$  are split by  $2\gamma_{\text{NV}}B_{\text{NV}}$  (with  $\gamma_{\text{NV}}=2.8$  MHz G<sup>-1</sup>) in a magnetic field  $B_{\text{NV}}$  applied along  $z$ . Hyperfine interactions between the NV's electron and <sup>14</sup>N nuclear spin ( $I=1$  and quantum number  $m_I$ ) further split the NV spin levels by an energy  $A_{\text{HF}}=2.18$  MHz into states  $|m_s, m_I\rangle$  (Fig. 1a)<sup>5</sup>. In our experiments, we use optical excitation and fluorescence detection to initialize and read out the NV spin<sup>18</sup> with a homebuilt confocal optical microscope<sup>9</sup> (Methods). Furthermore, we use microwave magnetic fields to perform optically detected electron spin resonance (ESR; Fig. 1b) and manipulate the NV's electronic spin states.

Coherent strain driving of NV spins is based on the sensitive response of the NV spin states to strain in the diamond host lattice. For uniaxial strain applied transverse to the NV axis, the corresponding strain-coupling Hamiltonian takes the form<sup>14</sup>

$$\hat{H}_{\text{str},\perp} = -\hbar\gamma_0^\perp (\hat{a} + \hat{a}^\dagger) (\hat{S}_+^2 + \hat{S}_-^2) \quad (1)$$

Here,  $\hbar$  is the reduced Planck constant,  $\gamma_0^\perp$  the transverse single-phonon strain-coupling strength and  $\hat{S}_{+(-)}$  and  $\hat{a}^\dagger(\hat{a})$  are the raising (lowering) operators for spin and phonons, respectively. Transverse strain thus leads to a direct coupling of the two electronic spin states  $|-1\rangle$  and  $|+1\rangle$  (ref. 9) and, in the case of near-resonant, time-varying (a.c.) strain, can coherently drive the transitions  $|-1, m_I\rangle \leftrightarrow |+1, m_I\rangle$  (ref. 8). For a classical (coherent) phonon field at frequency  $\omega_m/2\pi$ , equation (1) can be written as  $\hbar\Omega_m \cos(\omega_m t) (\hat{S}_+^2 + \hat{S}_-^2)$ , where  $\Omega_m = \gamma_0^\perp x_c/x_{\text{ZPF}}$  describes the amplitude of the strain drive, with  $x_{\text{ZPF}}$  and  $x_c$  the cantilever's zero-point fluctuation and peak amplitude, respectively (here, with  $x_{\text{ZPF}} \sim 7.7 \times 10^{-15}$  m and  $\gamma_0^\perp/2\pi \sim 0.08$  Hz, Supplementary Information). Interestingly, strain drives a dipole-forbidden transition ( $\Delta m_s = 2$ ), which would be difficult to access, for example, using microwave fields.

To generate and control a sizeable a.c. strain field for efficient coherent spin driving, we employed a mechanical resonator in the form of a singly clamped, single-crystalline diamond cantilever<sup>9</sup>, in which the NV centre is directly embedded (Fig. 1c and Methods). The cantilever was actuated at its mechanical resonance frequency  $\omega_m/2\pi = 6.83 \pm 0.02$  MHz using a piezo-element placed nearby the sample. We controlled the detuning between the mechanical oscillator and the  $|-1\rangle \leftrightarrow |+1\rangle$  spin transition by applying an adjustable external magnetic field  $B_{\text{NV}}$  along the NV axis (Fig. 1a and Methods).

<sup>1</sup>Department of Physics, University of Basel, Klingelbergstrasse 82, CH-4056 Basel, Switzerland. <sup>2</sup>Cavendish Laboratory, University of Cambridge, JJ Thomson Ave., Cambridge CB3 0HE, UK. <sup>†</sup>These authors contributed equally to this work. \*e-mail: patrick.maletinsky@unibas.ch

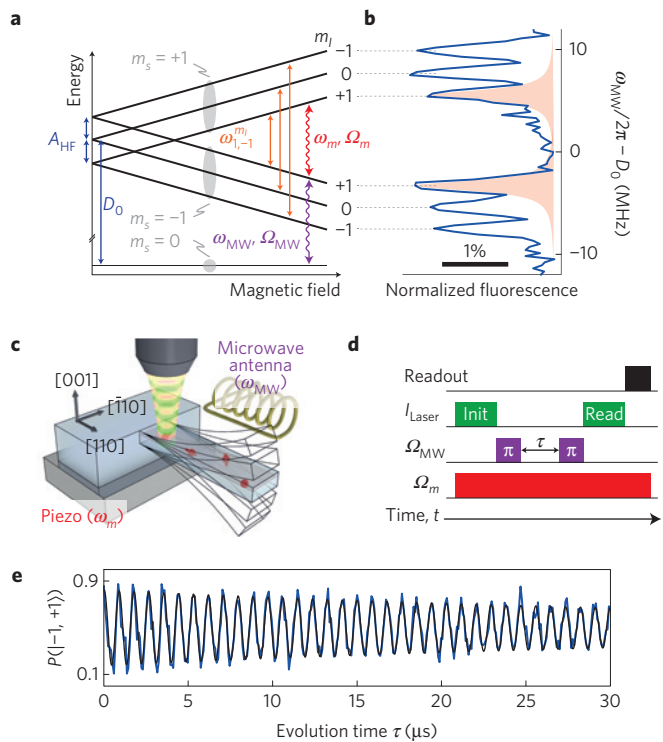


**Figure 1 | Experimental set-up and strain-induced coherent spin drive.** **a**, Energy levels of the NV spin as a function of magnetic field applied along the NV axis. Electronic spin states  $|m_s = \pm 1\rangle$  each split into three levels owing to hyperfine interactions with the NV's  $^{14}\text{N}$  nuclear spin ( $I=1$ ,  $A_{\text{HF}} = 2.18$  MHz). Wavy lines indicate strain (red) and microwave (violet) fields of frequency  $\omega$  and strength  $\Omega$ . **b**, Optically detected electron spin resonance of a single NV centre. **c**, Experimental set-up. NV spins (red) are coupled to a cantilever, which is resonantly driven at frequency  $\omega_m$  by a piezo-element. The NV spin is read out and initialized by green laser light and manipulated by microwave magnetic fields generated by a nearby antenna. **d**, Pulse sequence employed to observe strain-induced Rabi oscillations. **e**, Strain-driven Rabi oscillations. Data (blue) and a fit (black) to damped Rabi oscillations.

To demonstrate coherent NV spin manipulation using resonant a.c. strain fields, we first performed strain-driven Rabi oscillations between  $|-1\rangle$  and  $|+1\rangle$  for a given hyperfine manifold (here,  $m_l = 1$ ). To that end, we initialized the NV in  $|-1, 1\rangle$  by applying an appropriate sequence of laser and microwave pulses (Fig. 1d). We then let the NV spin evolve for a variable time  $\tau$ , under the influence of the coherent a.c. strain field generated by constantly exciting the cantilever at a fixed peak amplitude  $x_c \sim 100$  nm (Supplementary Information). After this evolution, we measured the resulting population in  $|-1, 1\rangle$  with a pulse sequence analogous to our initialization protocol. As expected, we observe strain-induced Rabi oscillations (Fig. 1e) for which we find a Rabi frequency  $\Omega_m/2\pi = 1.14 \pm 0.01$  MHz and hardly any damping over the 30  $\mu\text{s}$  observation time. Importantly, and in contrast to a recent study on NV ensembles<sup>8</sup>, this damping timescale is not limited by ensemble averaging, because our experiment was performed on a single NV spin.

We obtain further insight into the strength and dynamics of our coherent strain-driving mechanism from ESR spectroscopy of the strain-coupled NV spin states,  $|+1\rangle$  and  $|-1\rangle$ . For this, we employed a weak microwave tone at frequency  $\omega_{\text{MW}}/2\pi$  to probe the  $|0\rangle \leftrightarrow |\pm 1\rangle$  transitions as a function of  $B_{\text{NV}}$  in the presence of the coherent strain field (Fig. 2b). This field has a striking effect on the NV's ESR spectrum in that it induces excitation gaps

at  $\omega_{\text{MW}} - 2\pi D_0 = \pm\omega_m/2$ , that is, for  $B_{\text{NV}} \sim 0.9, 1.6$  and 2.3 G. At these values of  $B_{\text{NV}}$  the a.c. strain field in the cantilever is resonant with a given hyperfine transition, that is, the energy splitting  $\hbar\omega_{-1,-1}^{m_l}$  between  $|-1, m_l\rangle$  and  $|+1, m_l\rangle$  equals  $\hbar\omega_m$ . The energy gaps which we observe in the ESR spectra under resonant strain driving are evidence of the Autler–Townes (AT) effect—a prominent phenomenon in quantum electrodynamics<sup>19,20</sup>, which has previously been observed in atoms and molecules<sup>21</sup>, quantum dots<sup>22</sup> and superconducting qubits<sup>23</sup>. Our observation of the AT effect was performed on a single electronic spin in the microwave domain, and to the best of our knowledge constitutes the first observation of the AT effect under ambient conditions.

The observed AT splitting can be understood by considering the joint energetics of the NV spin states and the quantized strain field used to drive the spin<sup>20</sup> (Fig. 2a). The joint basis states  $|i; N\rangle$  consist of NV spin states  $|i\rangle$  dressed by  $N$  phonons in the cantilever. Strain couples  $|+1; N\rangle$  to  $|-1; N+1\rangle$  and leads to new eigenstates  $|\pm(N)\rangle$ , which anti-cross on resonance, where  $|\pm(N)\rangle = (|+1; N\rangle \pm |-1; N+1\rangle)/\sqrt{2}$  are split by an energy  $\hbar\Omega_m$ . As expected, this splitting increases linearly with the driving field amplitude (Fig. 2c), which we control through the strength of piezo excitation.

To investigate the limits of our coherent, strain-induced spin driving and study the resulting, strongly driven spin dynamics, we performed detailed dressed-state spectroscopy as a function of drive strength (Fig. 3a). To that end, we first set  $B_{\text{NV}}$  such that  $\omega_{-1,1}^{m_l=1} = \omega_m$  and then performed microwave ESR spectroscopy for different values of  $\Omega_m$ . For weak driving,  $\Omega_m \ll \omega_m$ , the dressed states emerging from the resonantly coupled states  $|-1, 1\rangle$  and  $|+1, 1\rangle$  split linearly with  $\Omega_m$ . The linear relationship breaks down for  $\Omega_m \gtrsim \omega_{-1,1}^{m_l=1}$  owing to multi-phonon couplings involving states which belong to different sub-spaces spanned by  $|\pm(N)\rangle$  and  $|\pm(M)\rangle$ , with  $N \neq M$  (ref. 20). This observation is closely linked to the breakdown of the rotating-wave approximation<sup>24</sup> and indicates the onset of the strong-driving regime we achieve in our experiment.

For even larger Rabi frequencies  $\Omega_m$ , the dressed states evolve into a characteristic sequence of crossings and anti-crossings. The (anti-)crossings occur in the vicinity of  $\Omega_m = q\omega_m$ , with  $q$  an odd (even) integer, and are related to symmetries of the Hamiltonian (1) (see ref. 20; Supplementary Information). Our experiment allows us to clearly identify the  $q=1$  and  $q=2$  (anti-)crossings (circles and crosses in Fig. 3a) and thereby demonstrates that we reside well within the strong-driving regime ( $\Omega_m > \omega_{-1,1}^{m_l}$ ) of a harmonically driven two-level system. We have carried out an extensive numerical analysis (Fig. 3b and Methods), which shows quantitative agreement with our experimental findings. For the largest values of  $\Omega_m$ , some discrepancies of the transition strengths between data and model remain; we tentatively assign these to uncertainties in microwave polarization, to possible variations of linewidths with  $\Omega_m$  and to our particular ESR detection scheme<sup>25</sup>. Our calculation further shows that, over our range of experimental parameters,  $\Omega_m$  is linear in  $x_c$  and reaches a maximum of  $\Omega_m^{\text{max}}/2\pi \sim 10.75$  MHz (at present limited by the maximally achievable piezo driving strength).

Continuous coherent driving can be employed to protect a quantum system from its noisy environment and thereby increase its coherence times<sup>12,26</sup>. For NV centre spins, decoherence is predominantly caused by environmental magnetic field noise<sup>5</sup>, which normally couples linearly to the NV spin through the Zeeman Hamiltonian  $H_Z = \gamma_{\text{NV}} S_z B_{\text{NV}}$  (Fig. 1a). Conversely, for the dressed states  $|\pm(N)\rangle$  we create by coherent strain driving,  $\langle \pm(N) | H_Z | \pm(N) \rangle = 0$  and the lowest-order coupling to magnetic fields is only quadratic (Fig. 2a). These states are thus less sensitive to magnetic field fluctuations and should exhibit increased coherence times relative to the undriven NV.

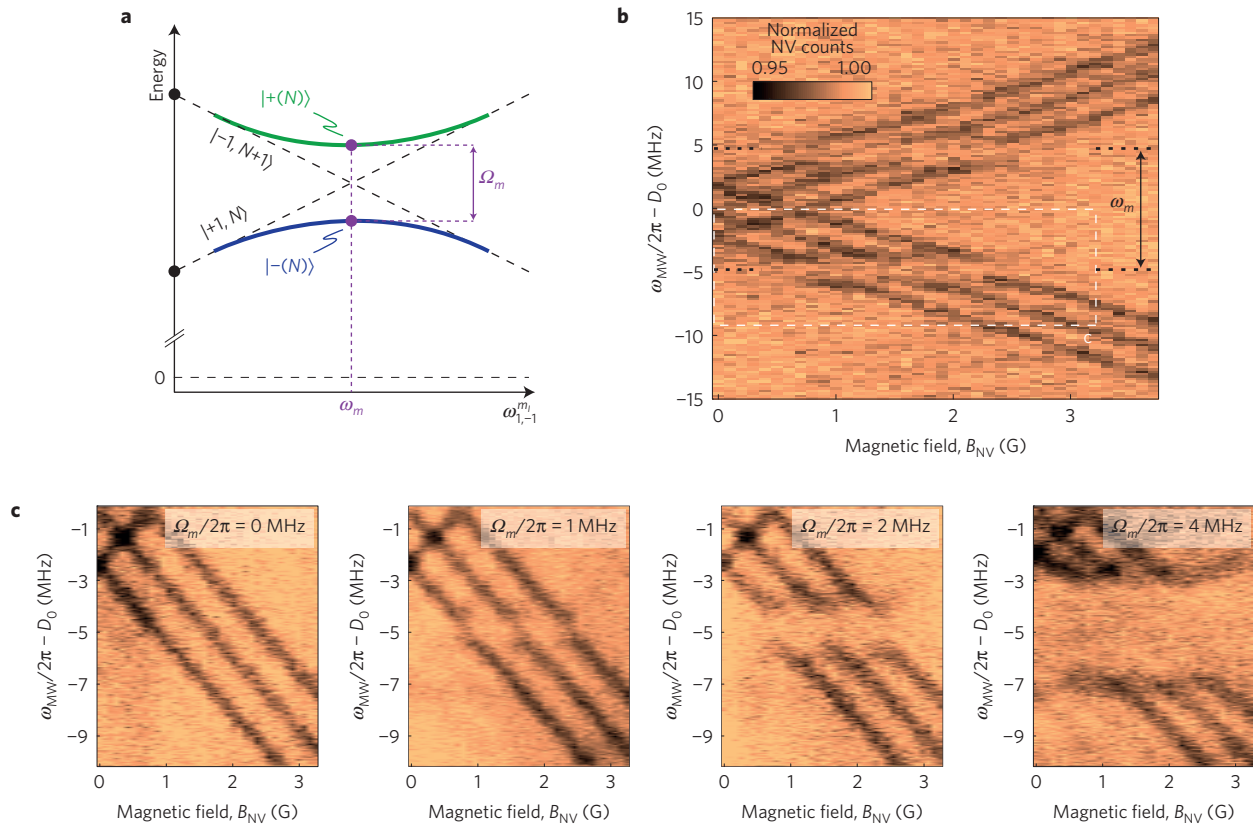


**Figure 2 | Mechanically induced Autler–Townes effect probed by microwave spectroscopy.** **a**, Eigenenergies of the joint spin–phonon system with basis states  $|m_s; N\rangle$  as a function of the spin splitting  $\omega_{1,-1}^{m_i}$ . Strain couples  $|1; N\rangle$  and  $| -1; N+1\rangle$  and, whenever the resonance condition  $\omega_{1,-1}^{m_i} = \omega_m$  is fulfilled, leads to new eigenstates  $|+(N)\rangle$  and  $|-(N)\rangle$  with energy splitting  $\hbar\Omega_m$  (see text). **b**, Microwave spectroscopy of phonon-dressed states using a weak microwave probe at  $\omega_{MW}$ . For  $m_i = -1, 0$  and  $1$ , resonance is separately established at  $B_{NV} \sim 0.9, 1.6$  and  $2.3$  G. **c**, Dependence of the energy gap between  $|+(N)\rangle$  and  $|-(N)\rangle$  on mechanical driving strength. As expected, the gap scales linearly with  $\Omega_m$  for each hyperfine state. Data was recorded over the parameter range indicated by white dashed lines in **b**.

To demonstrate such coherence enhancement by continuous driving<sup>12</sup>, we performed Ramsey spectroscopy on our strain-driven NV spin and compared the resulting dephasing times  $T_2^*$  against the undriven case (Fig. 4). For this, we adjusted  $B_{NV}$  such that  $\omega_{-1,1}^{m_i=1} = \omega_m$  and mechanically drove the NV with  $\Omega_m/2\pi = 1.68$  MHz to induce phonon-dressing of the NV. We then used pulsed microwaves<sup>25</sup> to perform Ramsey spectroscopy on the two Autler–Townes split dressed states emerging from  $|m_s = +1, m_i = +1\rangle$ . The resulting coherence signal (Fig. 4a) decays on a timescale of  $T_2^* = 16.4 \pm 0.6 \mu\text{s}$  and shows beating of two long-lived oscillations at  $0.63$  MHz and  $1.05$  MHz stemming from the two dressed states we address (Supplementary Information). Compared to the bare NV dephasing time of  $T_2^* = 3.6 \pm 0.1 \mu\text{s}$  (Fig. 4b), this demonstrates a significant enhancement of  $T_2^*$  caused by our continuous, mechanical drive.

Although our protocol decouples NVs from magnetic field noise, it renders them vulnerable to fluctuations in electric field and strain. Most importantly, shallow NVs experience excess dephasing from fluctuating surface electric fields<sup>27</sup>, which are likely to dominate the residual dephasing we observe. Additional dephasing mechanisms of lesser relevance to our experiment include cantilever thermal noise (Supplementary Information) or second-order couplings<sup>28</sup> of magnetic fields to the NV. Our decoupling protocol is readily tunable: for increasing  $\Omega_m$ , we have observed an initially monotonic, approximately linear increase of  $T_2^*$  (Supplementary Information), which saturates for  $\Omega_m/2\pi \gtrsim 1$  MHz. We assign this current limitation to the onset of technical noise<sup>12</sup>, whose mitigation might lead to further improvements of  $T_2^*$  in the future. Furthermore,

tunability offers interesting perspectives to systematically study the still largely unexplored, electric-field-induced dephasing processes for shallow NVs.

Our approach to strong coherent strain driving of a single electronic spin will have implications far beyond the coherence protection and dressed-state spectroscopy that we have demonstrated in this work. By combining our strain drive with coherent microwave spin manipulation, our NV spin forms an inverted three-level ‘ $\Delta$ ’-system, on which all three possible spin transitions can be coherently addressed. This setting is known to lead to unconventional spin dynamics<sup>29</sup>, which here could be observed on a single, highly coherent spin and exploited for sensing and quantum manipulation of our hybrid device. Strain-induced a.c. Stark shifts can furthermore be employed to dynamically tune<sup>30</sup> the energies of the NV hyperfine states—an attractive perspective for the use of  $^{14}\text{N}$  nuclear spins as quantum memories<sup>5</sup>. The decoherence protection by continuous strain driving that we have demonstrated will have an impact for any quantum technology where pulsed decoupling protocols cannot be employed (such as d.c. electric field sensing). Further studies of the remaining decoherence processes under mechanical driving, which remain largely unexplored until now, offer another exciting avenue to be pursued in the future. On a more far-reaching perspective, our experiments lay the foundation for exploiting diamond-based hybrid spin-oscillator systems for quantum information processing and sensing, where our system forms an ideal platform for implementing proposed schemes for spin-induced phonon cooling and lasing<sup>31</sup> or oscillator-induced spin squeezing<sup>14</sup>.

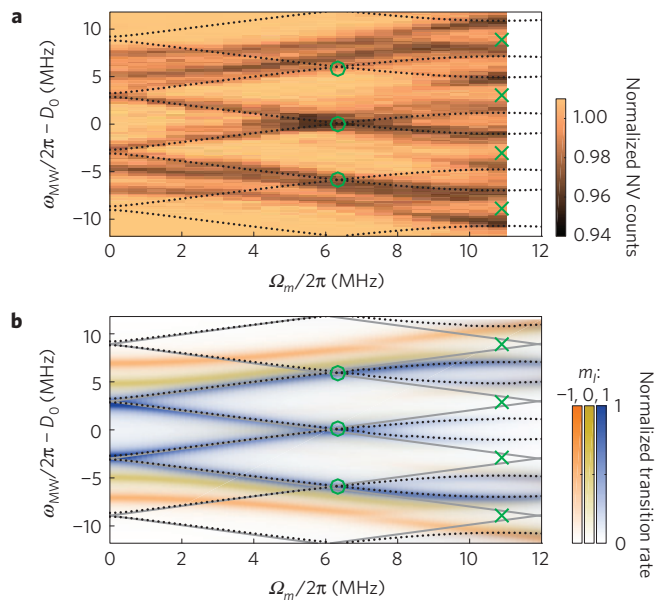


**Figure 3 | Dressed-state spectroscopy of the strongly driven NV spin.**

**a**, Microwave spectroscopy of the mechanically driven NV spin at  $B_{NV} = 1.8$  G (where  $\omega_m = \omega_{1,-1}^{m_l=+1}$ ) as a function of drive strength  $\Omega_m$ . The resonantly coupled states ( $|\pm 1, +1\rangle$ ) at  $\omega_{MW}/2\pi - D_0 = \pm 2.98$  MHz first split linearly with  $B_{NV}$  and then evolve into a sequence of crossings and anti-crossings (green circles and crosses, respectively) with higher-order dressed states, indicative of the strong-driving regime. **b**, Calculated transition rates from  $|m_s = 0\rangle$  to the dressed states obtained by Fermi's golden rule (Methods). Blue, green and orange shaded transitions correspond to the hyperfine manifolds  $m_l = +1, 0$  and  $-1$ , respectively. In both panels, black dots indicate the calculated dressed-state energies for  $m_l = +1$ . Grey lines in **b** show the same under the rotating-wave approximation. Deviations between black dots and the grey lines therefore indicate the onset of the strong-driving regime.

## Methods

Methods and any associated references are available in the [online version of the paper](#).

Received 7 March 2015; accepted 24 June 2015; published online 3 August 2015

## References

- Nielsen, M. A. & Chuang, I. L. *Quantum Computation and Quantum Information* (Cambridge Univ. Press, 2000).
- Nadj-Perge, S., Frollov, S. M., Bakkers, E. P. A. M. & Kouwenhoven, L. P. Spin-orbit qubit in a semiconductor nanowire. *Nature* **468**, 1084–1087 (2010).
- Clarke, J. & Wilhelm, F. K. Superconducting quantum bits. *Nature* **453**, 1031–1042 (2008).
- Hanson, R., Kouwenhoven, L. P., Petta, J. R., Tarucha, S. & Vandersypen, L. M. K. Spins in few-electron quantum dots. *Rev. Mod. Phys.* **79**, 1217–1265 (2007).
- Dobrovitski, V., Fuchs, G., Falk, A., Santori, C. & Awschalom, D. Quantum control over single spins in diamond. *Ann. Rev. Condens. Matter Phys.* **4**, 23–50 (2013).
- Oliver, W. D. *et al.* Mach-Zehnder interferometry in a strongly driven superconducting qubit. *Science* **310**, 1653–1657 (2005).
- London, P., Balasubramanian, P., Naydenov, B., McGuinness, L. P. & Jelezko, F. Strong driving of a single spin using arbitrarily polarized fields. *Phys. Rev. A* **90**, 012302 (2014).
- MacQuarrie, E. R. *et al.* Coherent control of a nitrogen-vacancy center spin ensemble with a diamond mechanical resonator. *Optica* **2**, 233–238 (2015).
- Teissier, J., Barfuss, A., Appel, P., Neu, E. & Maletinsky, P. Strain coupling of a nitrogen-vacancy center spin to a diamond mechanical oscillator. *Phys. Rev. Lett.* **113**, 020503 (2014).

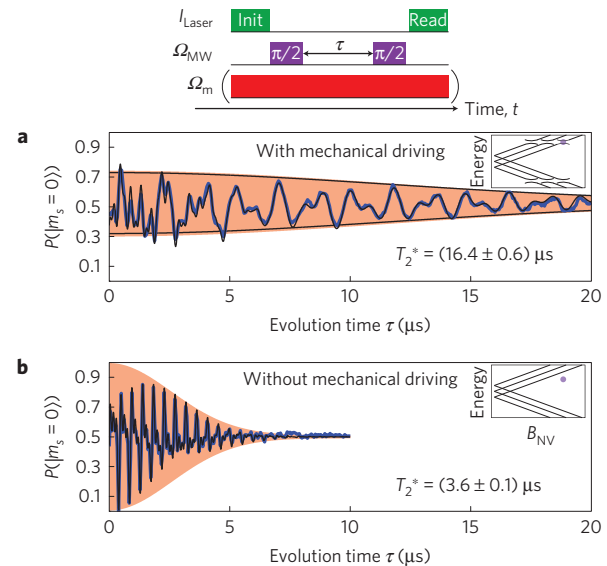


**Figure 4 | Protecting NV spin coherence by coherent strain driving.** **a**, Spin coherence decay of  $|\pm(N)\rangle$  (for  $m_l = +1$ ) as measured by Ramsey interferometry between the state  $|m_s = 0\rangle$  and the  $|m_s = +1\rangle$  manifolds using the pulse sequence depicted on the top. The probability for the NV to occupy the  $|m_s = 0\rangle$  manifold after the sequence is denoted as  $P(|m_s = 0\rangle)$ . The inset illustrates the NV spin's eigenenergies as a function of  $B_{NV}$  and indicates the magnetic field and microwave frequencies employed (purple dot) with respect to the dressed-state spectrum shown in Fig. 2b. **b**, Measurement of NV spin coherence time in the undriven case, as determined by Ramsey spectroscopy between  $|m_s = 0\rangle$  and  $|m_s = +1\rangle$ , in the absence of mechanical driving. Inset as in **a**. In both panels, the orange envelope indicates the coherence decay extracted from our fit.

- Ovartchaiyapong, P., Lee, K. W., Myers, B. A. & Jayich, A. C. B. Dynamic strain-mediated coupling of a single diamond spin to a mechanical resonator. *Nature Commun.* **5**, 4429 (2014).
- Silveri, M., Tuorila, J., Kemppainen, M. & Thuneberg, E. Probe spectroscopy of quasienergy states. *Phys. Rev. B* **87**, 134505 (2013).
- Xu, X. *et al.* Coherence-protected quantum gate by continuous dynamical decoupling in diamond. *Phys. Rev. Lett.* **109**, 070502 (2012).
- Danon, J. & Rudner, M. S. Multilevel interference resonances in strongly driven three-level systems. *Phys. Rev. Lett.* **113**, 247002 (2014).
- Bennett, S. D. *et al.* Phonon-induced spin-spin interactions in diamond nanostructures: Application to spin squeezing. *Phys. Rev. Lett.* **110**, 156402 (2013).
- Gustafsson, M. V. *et al.* Propagating phonons coupled to an artificial atom. *Science* **346**, 207–211 (2014).
- Wilson-Rae, I., Zoller, P. & Imamoglu, A. Laser cooling of a nanomechanical resonator mode to its quantum ground state. *Phys. Rev. Lett.* **92**, 075507 (2004).
- MacQuarrie, E. R., Gosavi, T. A., Jungwirth, N. R., Bhawe, S. A. & Fuchs, G. D. Mechanical spin control of nitrogen-vacancy centers in diamond. *Phys. Rev. Lett.* **111**, 227602 (2013).
- Gruber, A. *et al.* Scanning confocal optical microscopy and magnetic resonance on single defect centers. *Science* **276**, 2012–2014 (1997).
- Autler, S. H. & Townes, C. H. Stark effect in rapidly varying fields. *Phys. Rev.* **100**, 703–722 (1955).
- Cohen-Tannoudji, C., Dupont-Roc, J. & Grynberg, G. *Atom-Photon Interactions: Basic Processes and Applications* (Wiley, 1992).
- Wrigge, G., Gerhardt, I., Hwang, J., Zumofen, G. & Sandoghdar, V. Efficient coupling of photons to a single molecule and the observation of its resonance fluorescence. *Nature Phys.* **4**, 60–66 (2008).
- Xu, X. *et al.* Coherent optical spectroscopy of a strongly driven quantum dot. *Science* **317**, 929–932 (2007).
- Baur, M. *et al.* Measurement of Autler-Townes and Mollow transitions in a strongly driven superconducting qubit. *Phys. Rev. Lett.* **102**, 243602 (2009).
- Fuchs, G. D., Dobrovitski, V. V., Toyli, D. M., Heremans, F. J. & Awschalom, D. D. Gigahertz dynamics of a strongly driven single quantum spin. *Science* **326**, 1520–1522 (2009).
- Dreau, A. *et al.* Avoiding power broadening in optically detected magnetic resonance of single NV defects for enhanced dc magnetic field sensitivity. *Phys. Rev. B* **84**, 195204 (2011).

26. Timoney, N. *et al.* Quantum gates and memory using microwave-dressed states. *Nature* **476**, 185–188 (2011).
27. Dolde, F. *et al.* Electric-field sensing using single diamond spins. *Nature Phys.* **7**, 459–463 (2011).
28. Ithier, G. *et al.* Decoherence in a superconducting quantum bit circuit. *Phys. Rev. B* **72**, 134519 (2005).
29. Buckle, S., Barnett, S., Knight, P., Lauder, M. & Pegg, D. Atomic interferometers. *Opt. Acta* **33**, 1129–1140 (1986).
30. Jundt, G., Robledo, L., Högele, A., Fält, S. & Imamoglu, A. Observation of dressed excitonic states in a single quantum dot. *Phys. Rev. Lett.* **100**, 177401 (2008).
31. Keesidis, K. V., Bennett, S. D., Portolan, S., Lukin, M. D. & Rabl, P. Phonon cooling and lasing with nitrogen-vacancy centers in diamond. *Phys. Rev. B* **88**, 064105 (2013).

### Acknowledgements

We thank V. Jacques for fruitful discussions, P. Appel for initial assistance with nanofabrication and L. Thiel for support with the experiment control software. We

gratefully acknowledge financial support from SNI; NCCR QSIT; SNF grants 200021\_143697; and EU FP7 grant 611143 (DIADEMS). A.N. holds a University Research Fellowship from the Royal Society and acknowledges support from the Winton Programme for the Physics of Sustainability.

### Author contributions

A.B. and J.T. carried out the experiment and analysed the data. E.N. provided essential support in sample fabrication. A.N. provided theoretical support and modelled the data. All authors commented on the manuscript. P.M. wrote the manuscript, conceived the experiment and supervised the project.

### Additional information

Supplementary information is available in the [online version of the paper](#). Reprints and permissions information is available online at [www.nature.com/reprints](http://www.nature.com/reprints). Correspondence and requests for materials should be addressed to P.M.

### Competing financial interests

The authors declare no competing financial interests.

## Methods

**Sample fabrication.** Our cantilevers consist of single-crystalline, ultra-pure [001]-oriented diamond (Element Six, 'electronic grade'), are aligned with the [110] crystal direction and have dimensions in the range of  $(0.2-1) \times 3.5 \times (15-25) \mu\text{m}^3$  for thickness, width and length, respectively. The fabrication process is based on recently established top-down diamond nanofabrication techniques<sup>32</sup>. In particular, we use electron beam lithography at 30 keV to pattern etch masks for our cantilevers into a negative tone electron beam resist (FOX-16 from Dow Corning, spun to a thickness of  $\sim 500$  nm onto the sample). The developed pattern directly acts as an etch mask and is transferred into the diamond surface using an inductively coupled plasma reactive ion etcher (ICP-RIE, Sentech SI 500). To create cantilevers with vertical sidewalls, we use a plasma containing 50% argon and 50% oxygen (gas flux 50 sccm each). The plasma is run at 1.3 Pa pressure, 500 W ICP source power and 200 W bias power. NV centres in our cantilevers were created before nanofabrication by <sup>14</sup>N ion implantation with dose, energy and sample tilt of  $10^{10} \text{ cm}^{-2}$ , 12 keV and  $0^\circ$ , respectively. Based on numerical simulations (using the 'SRIM' software package), this yields an estimated implantation depth of  $\sim 17$  nm. To create NV centres, we annealed our samples at high vacuum ( $\lesssim 10^{-6}$  mbar) in a sequence of temperature steps at 400 °C (4 h), 800 °C (2 h) and 1,200 °C (2 h).

**Experimental set-up.** Experiments are performed in a homebuilt confocal microscope set-up at room temperature and at atmospheric pressure. A 532 nm laser (NovaPro 532-300) is coupled into the confocal system through a dichroic mirror (Semrock LM01-552-25). A microscope objective (Olympus XMFLN40x) is used to focus the laser light onto the sample, which is placed on a micropositioner (Attocube ANSxyz100). Red fluorescence photons are collected by the same microscope objective, transmitted through the dichroic mirror and coupled into a single-mode optical fibre (Thorlabs SM600), which acts as a pinhole for confocal detection. Photons are detected using an avalanche photodiode (Laser Components Count-250C) in Geiger mode. Scan control and data acquisition (photon counting) are achieved using a digital acquisition card (NI-6733). The microwave signal for spin manipulation is generated by a SRS SG384 signal generator, amplified by a Minicircuit ZHL-42W+ amplifier and delivered to the sample using a homebuilt near-field microwave antenna. Laser, microwave and detection signals were gated using microwave switches (Minicircuit Switch ZASWA-2-50DR+), which were controlled through digital pulses generated by a fast pulse generator (SpinCore PulseBlasterESR-PRO). Gating of the laser is achieved using a double-pass acoustic optical modulator (Crystal Technologies 3200-146). Mechanical excitation of the cantilevers was performed with a piezoelectric element placed directly below the sample. The excitation signal for the piezo was generated with a signal generator (Agilent 3320A). A three-axis magnetic field was generated by three homebuilt coil pairs driven by constant-current sources (Agilent E3644A).

**Measurement procedure and error bars.** ESR measurements were performed using a pulsed ESR scheme<sup>25</sup>, where the NV spin is first initialized in

$|m_s = 0\rangle$  using green laser excitation, then driven by a short microwave ' $\pi$ -pulse' of length  $\tau$  (that is, a pulse such that  $2\pi\Omega_{\text{MW}}\tau = \pi$ ) and finally read out using a second green laser pulse. Compared to conventional, continuous-wave ESR, this scheme has the advantage of avoiding power broadening of the ESR lines by green laser light and was therefore employed throughout this work.

Our experiments were performed on three different NV centres in three different cantilevers: data in Figs 1 and 4 were obtained on NV #1, whereas Figs 2 and 3 were recorded on NVs #2 and #3, respectively. NVs #1–3 all showed slightly different values of  $D_0$  owing to variations in static local strain and transverse magnetic fields. The zero-field splittings for these three NVs were  $D_0 = 2.870$  GHz, 2.871 GHz and 2.8725 GHz, respectively. The values of  $\omega_m$  for the cantilevers of NVs #1–3 were  $\omega_m/2\pi = 6.83, 9.18$  and 5.95 MHz, respectively.

Throughout this paper, errors represent 95% confidence intervals for the nonlinear least-squares parameter estimates to our experimental data. The only exception is the mechanical resonance frequency  $\omega_m$ , where error bars represent the linewidth of the cantilever resonance curves, which we measured optically in separate experiments. The actual error bars in determining  $\omega_m$  are significantly smaller than the linewidth and do not influence the findings presented in this paper.

**Simulations.** Following ref. 11 we employ Floquet theory to treat the time dependence of the strain-induced spin driving,  $\hat{H}_m = \hbar\Omega_m \cos \omega_m t (\hat{S}_x^2 + \hat{S}_y^2)$ , beyond the rotating-wave approximation (RWA), as it is expected to break down in the strong-driving limit  $\Omega_m > \omega_{m_i=1}^{\text{max}}$ . The key idea here is to map the Hamiltonian with periodic time dependence on an infinite-dimensional, but time-independent Floquet Hamiltonian  $\mathcal{H}_F$ . We can then solve the eigenvalue problem  $\mathcal{H}_F|u_i\rangle = \hbar\omega_i|u_i\rangle$  with standard methods to obtain quasi-energies  $\hbar\omega_i$  and corresponding eigenvectors  $|u_i\rangle$ .

Treating the weak microwave drive up to second order in drive strength we find the rate for the system to leave the initial state with Fermi's golden rule as<sup>11</sup>

$$\mathcal{P} = \frac{1}{\hbar^2} \sum_{if} \frac{\gamma_f |\langle u_f | \hat{H}_{\text{MW}} | u_i \rangle|^2}{(\omega_f - \omega_i - \omega_{\text{MW}})^2 + \frac{\gamma_f^2}{4}}$$

where the sum over  $i$  and  $f$  runs over all the eigenstates of the Floquet Hamiltonian and the microwave driving Hamiltonian is  $\hat{H}_{\text{MW}} = \sum_{m_f} \hbar\Omega_{\text{MW}} (|+1, m_f\rangle \langle 0, m_f| + |-1, m_f\rangle \langle 0, m_f| + \text{H.c.})$  with drive frequency  $\Omega_{\text{MW}}$ , assuming a linearly polarized microwave field. For the simulations shown in Fig. 3b we assumed an initial state  $|u_i\rangle = |m_s = 0, m_f\rangle$  and linewidths  $\gamma_f = \gamma = 1$  MHz, and summed the result incoherently over all nuclear spin quantum numbers  $m_f \in \{-1, 0, 1\}$ .

## References

- Maletinsky, P. *et al.* A robust scanning diamond sensor for nanoscale imaging with single nitrogen-vacancy centres. *Nature Nanotech.* **7**, 320–324 (2012).